
A Soft X-Ray Lag Detected in Centaurus A

Yutaro Tachibana ¹, Taiki Kawamuro ², Yoshihiro Ueda ², Megumi Shidatsu ³, Makoto Arimoto ¹, Taketoshi Yoshii ¹, Yoichi Yatsu ¹, Yoshihiko Saito ¹, Sean Pike ⁴, and Nobuyuki Kawai ¹

¹Department of Physics, Tokyo Institute of Technology, 2-12-1, Ohokayama, Tokyo, Japan

²Department of Astronomy, Kyoto University, Oiwake-cho, Sakyo-ku, Kyoto 606-8502, Japan

³MAXI team, Institute of Physical and Chemical Research, Wako, Saitama 351-0198, Japan

⁴Department of Physics, Brown University, Providence, Rhode Island 02912, USA

*E-mail: E-mail : tachibana@hp.phys.titech.ac.jp

Received; Accepted

Abstract

We performed time lag analysis on the X-ray light curves of Centaurus A (Cen A) obtained by the Gas Slit Camera (GSC) aboard the Monitor of All-sky X-ray Image (*MAXI*) in three energy bands (2–4 keV, 4–10 keV, and 10–20 keV). We discovered a soft X-ray lag relative to higher energies (soft lag) on a time scale of days by employing the discrete correlation function (DCF) and the z-transformed discrete correlation function (ZDCF) method in a flare episode. A peak in the DCF and the ZDCF was observed at a soft lag of ~ 5 days in 2–4 keV versus 4–10 keV and in 4–10 keV versus 10–20 keV, and ~ 10 days in 2–4 keV versus 10–20 keV. We found it difficult to explain the observed X-ray variation with the one-zone synchrotron self-Compton (SSC) model, in which the soft lags reflect the different cooling times of the relativistic electrons in these three energy bands. Alternatively, if the X-ray variation was produced in a corona surrounding or along the inner part of the accretion disk, we can explain this phenomenon due to different Compton cooling times of the electrons with different energies.

Key words:

1 Introduction

Centaurus A (Cen A, NGC 5128), at a distance of 3.8 Mpc (Harris et al. 2010), is the nearest active galactic nuclei (AGN) from the Milky Way galaxy and is known as the brightest Seyfert galaxy in the X-ray sky (2.87×10^{-10} erg cm $^{-2}$ s $^{-1}$ in the 4–10 keV band; Hiroi et al. 2011, and 7.48×10^{-10} erg cm $^{-2}$ s $^{-1}$ in the 14–195 keV band; Tueller et al. 2008). In addition, this object has often been considered as a jet-dominated AGN seen from the side called “misdirected BL Lac object” (Morganti et al. 1992; Chiaberge et al. 2001) with its jet inclined to the viewing angle at $\gtrsim 50^\circ$ (Tingay et al. 1998). Owing to its brightness and proximity, this object has been an ideal target to study the geometry and the emission mechanism around a supermassive black hole.

Despite astronomers’ efforts, however, the origin of the X-ray radiation from Cen A has not been easily identified from its energy spectrum. The observed X-ray spectrum has no significantly different features from typical Seyfert galaxies, which radiate X-rays mainly from the inner disk region with Comptonization in hot plasmas located above or around the accretion disk (*e.g.* Rothschild et al. 1999; Beckmann et al. 2011; Fukazawa et al. 2011). On the other hand, the high energy tail of the X-ray spectrum appears to be smoothly connected to the MeV emission which is believed to be generated from a jet, and the spectral energy distribution (SED) in the energy range between radio and GeV γ -ray can be modeled successfully by the one-zone SSC model or other varieties of jet emission models (*e.g.* Abdo et al. 2010b; Roustazadeh & Böttcher 2011; Petropoulou et al. 2013), though a combination of a thermal inverse Compton component and a non-thermal jet emission also describe the SED equally well (Abdo et al. 2010b).

When the spectral analysis does not provide a unique emission mechanism of AGNs, time variability analysis, especially time lag analysis, may be useful to resolve the issue. Kataoka et al. (2000) detected soft lags (*i.e.* the variation in a lower energy band lags respect to that of a higher energy band) on a time scale of $\sim 10^3$ – 10^4 sec in an X-ray flare from the TeV blazar PKS 2155-304 and estimated the magnetic field strength at the X-ray emitting region in the jet with the hypothesis that the delays are caused by different synchrotron lifetimes of the relativistic electrons. Similar discussion was presented by Tanihara et al. (2001) for other blazar objects: Mrk 421 and Mrk 501. Sriram et al. (2009), conversely, found hard lags (vice versa for soft lag) on a time scale of $\sim 10^2$ – 10^3 sec in the Seyfert 1 galaxy NGC 4593 using the *XMM-Newton*/EPIC. The authors interpreted the hard lags as time scale of thermal Compton scattering in a compact central corona and derived its size as about five Schwarzschild radii for the black hole mass $7 \times 10^6 M_\odot$. Recently, De Marco et al. (2013), based on the study of 32 radio quiet AGNs, discovered the relation between black hole masses (M_{BH}) and soft X-ray lags ($\tau \approx 10$ –600 sec) in high-frequency variation ($\nu \approx 0.07$ – 4×10^{-3}

Hz); $\log|\tau| = 1.98[\pm 0.08] + 0.59[\pm 0.11]\log(M_{\text{BH}}/10^7 M_{\odot})$.

For Cen A, time lag analysis in the X-ray band has scarcely been applied as yet, presumably because of remarkably stable spectral (or flux) behavior as reported by Rothschild et al. (2011) based on 12.5-year observation by the *Rossi Timing X-ray Explorer* combined with pointed observation with inadequate time coverage or continuous monitoring with insufficient sensitivity in the X-ray band. The *Monitor of All-sky X-ray Image (MAXI)*; Matsuoka et al. 2009), launched in August 2009, has a high sky coverage of 95% and a X-ray sensitivity to detect above 15 mCrab in the 4–10 keV band with a cadence of ~ 90 min (Sugizaki et al. 2011), thus allowing us to investigate a long-term activity for AGNs with a sufficient time resolution.

In this paper, to study X-ray variation properties in Centaurus A, we focused on a flare-like enhancement observed in X-ray light curves during MJD = 55075–55160 obtained by *MAXI/GSC*. First, we present the results of time lag analysis by employing the discrete correlation function (DCF; Edelson & Krolic, 1988) and the z-transformed discrete correlation function (ZDCF; Alexander, 1997). Next, we show the results of flare profile fitting to consider which feature in the light curves contributes to the detected soft lags. Finally, we discuss the interpretations of this phenomenon and the origin of X-ray emission of Cen A based on our analysis results.

2 Observations and Light Curves

In August 2009, the *MAXI* was launched and attached to the Japanese experiment module “Kibo” on the *International Space Station (ISS)*. Since then, the gas slit camera (GSC; Mihara et al. 2011) and solid-state slit camera (SSC; Tomida et al. 2011) aboard *MAXI* has been producing all sky X-ray image at every orbital period of *ISS* (92 minutes). The SSC employs X-ray CCD arrays and covers the energy range from 0.5 keV to 12 keV, while, the GSC employs gas proportional counters and covers the energy range from 2 keV to 20 keV. In this paper, we use the 2–4 keV, 4–10 keV, and 10–20 keV light curves of Cen A obtained by the *MAXI/GSC*, with the following data selection criteria and the background model described in Hiroi et al. (2013). We excluded the event data taken at high latitude regions ($|\text{latitude}| > 40^\circ$), where the charged particle radion is high, and those detected in near both ends of each proportional counter at a photon incident angle $|\phi| > 38^\circ$ (for the definition of ϕ , see Mihara et al. 2011) where the background rejection efficiency is lower.

Figure 1 shows the light curve of Cen A during MJD=55075–55160 in the three energy bands. Calculated fluxes binned per day are represented as black filled circles. Particularly as is evidently in the light curve in the 4–10 keV band, flare-like activity was observed in the X-ray band from MJD \sim 55090 to MJD \sim 55130, and the peak flux of ~ 60 mCrab is the highest value ever since the

beginning of the *MAXI*/GSC observation of this object. The amplitudes of flux enhancements (a factor of ~ 2) are very similar in the three energy bands. On the other hand, the temporal variability looks somewhat different among the three energy bands. The flare decay time in 2–4 keV seems longer than those in the other energy bands, while, the flare rise time and the time scale of variation in 10–20 keV seems shorter than those in the other energy bands (see also §4.2).

3 Method of Time Lag Analysis

To evaluate time lags in X-ray variation between two different energy bands, we employed two techniques based on the discrete correlation function, called the continuously evaluated discrete correlation function and the z-transformed discrete correlation function.

3.1 Discrete correlation function

The DCF was introduced by Edelson and Krolic (1988). To analyze the irregularly sampled astronomical data, DCF has been used widely to uncover correlations or lags between flux variations in two different energy bands, especially for AGNs. This function provides the correlation coefficient between two unevenly sampled time-series data as a function of lag (τ_{lag}), and the value τ_{lag} , corresponding to the maximum correlation or the centroid of $DCF(\tau_{\text{lag}})$, is presumed to be the value of the lag in the variations in two time series. First, we calculate the set of un-binned discrete correlation functions (UDCFs) for all measured pairs (a_i, b_j) defined as follows:

$$UDCF_{ij} = \frac{a_i - \bar{a}}{\sigma_a} \times \frac{b_j - \bar{b}}{\sigma_b}, \quad (1)$$

where \bar{a} and \bar{b} are the means, and σ_a and σ_b are the standard deviation of data sets a and b . Each $UDCF_{ij}$ is associated with the pairwise lag $\Delta t_{ij} = t_j - t_i$. Next, we average the M pairs for which over $\tau_{\text{lag}} - \Delta\tau_{\text{lag}}/2 \leq \Delta t_{ij} < \tau_{\text{lag}} + \Delta\tau_{\text{lag}}/2$,

$$DCF(\tau_{\text{lag}}) = \frac{1}{M} \sum_{ij} UDCF_{ij}. \quad (2)$$

One σ error of each bin is defined by the following expression:

$$\sigma(\tau_{\text{lag}}) = \frac{1}{M-1} \left[\sum_{ij} (UDCF_{ij} - DCF(\tau_{\text{lag}}))^2 \right]^{1/2}. \quad (3)$$

3.2 Continuously evaluated discrete correlation function

The continuously evaluated discrete correlation function (CEDCF) was introduced by Goicoechea et al. (1998). The CEDCF is an oversampled DCF, meaning that the bin-to-bin interval is smaller than the bin width, and thus this method allows us to determine more precise time lags from the position

of the peak or centroid than via the standard DCF method. Details of advantages of this method are described in Gil-Merino et al. (2002). Here, we used the centroid instead of the peak lag, because the centroid is less sensitive to a particular binning used and statistical fluctuation. In order to estimate the significance and uncertainties of the time lags, we built a cross-correlation centroid distribution (CCCD) by running Monte-Carlo simulations known as “flux randomization/random subset selection” (FR/RSS) described in detail by Peterson et al. (1998), which yields conservative uncertainties in the obtained lags. Here, we calculated the centroid of the CEDCF as $(\sum_i \tau_i CEDCF_i) / (\sum_i CEDCF_i)$ for all points which have a correlation coefficient close to the peak ($CEDCF_i \geq 0.8 \times CEDCF_{peak}$). In each simulation, a centroid and a peak of CEDCF are determined and recorded by the manner as described above. We can also obtain τ_{median} and $\pm \Delta\tau_{68}$ directly from the constructed CCCD respectively. The obtained values of $\pm \Delta\tau_{68}$ correspond to 1σ errors for a normal distribution.

3.3 Z-transformed discrete correlation function

Alexander (1997) proposed the z-transformed discrete correlation function (ZDCF) to improve the CCF analysis of sparse and unevenly sampled light curves. Several biases of the conventional DCF method can be corrected by the ZDCF technique by using Fisher’s z-transform and equal population binning rather than equal time interval $\Delta\tau_{\text{lag}}$. If we have n pairs in a given time lag τ_{lag} , the correlation coefficient at this lag $r(\tau_{\text{lag}})$ is estimated by

$$r(\tau_{\text{lag}}) = \frac{1}{n-1} \sum_{ij} \left(\frac{a_i - \bar{a}}{\sigma_a} \times \frac{b_j - \bar{b}}{\sigma_b} \right), \quad (4)$$

where \bar{a}, \bar{b} and σ_a, σ_b are the means and the standard deviations of data sets a and b , respectively. The sampling distribution of r is highly skewed (*i.e.*, the distribution is far from normal distribution), and therefore calculating its sampling error by simple standard variance of r might be very inaccurate. Assuming a and b are drawn from the bivariate normal distribution, we can transform r into an approximately normally distributed random variable by Fisher’s z :

$$z = \frac{1}{2} \log \left(\frac{1+r}{1-r} \right), \quad \rho = \tanh z, \quad \zeta = \frac{1}{2} \log \left(\frac{1+\rho}{1-\rho} \right). \quad (5)$$

The mean and the variance of z are approximately equal to

$$\bar{z} = \zeta + \frac{\rho}{2(n-1)} \times \left[1 + \frac{5+\rho^2}{4(n-1)} + \frac{11+2\rho^2+3\rho^4}{8(n-1)^2} + \dots \right], \quad (6)$$

$$s_z^2 = \frac{1}{n-1} \left[1 + \frac{4-\rho^2}{2(n-1)} + \frac{22-6\rho^2-3\rho^4}{6(n-1)^2} + \dots \right]. \quad (7)$$

These relations yield the interval corresponding to the $\pm 1\sigma$ error interval which is represented as

$$\delta r_{\pm} = |\tanh(\bar{z} \pm s_z) - \rho|. \quad (8)$$

The binning is performed according to equal population rather than equal $\Delta\tau_{\text{lag}}$, where each bin contains at least $n_{\text{min}} = 11$ points (for a meaningful statistical interpretation). Also, the interdependent pairs are discarded in each bin, namely a new pair whose a or b points have previously appeared in that bin is not gathered anymore. It is more robust method than conventional DCF method when the light curves are very sparsely and irregularly sampled. The ZDCF time lag is characterized by the centroid τ_{cent} , which can be calculated through the same procedure as that of CEDCF.

4 Analysis and Result

4.1 Time lags between the light curves

Using the method of the time lag analysis based on the DCF described in §3, we investigated the correlations and time lags of the obtained X-ray fluctuations among three energy bands during the flare observed at MJD ~ 55090 . The CEDCFs and the ZDCFs between 2–4 keV and 4–10 keV, 4–10 keV and 10–20 keV, and 2–4 keV and 10–20 keV are shown in Figure 2. The CEDCFs calculated with a bin size of 2 days and a distance between centers of bins of 1 day are shown by shadowed areas, and the data points and the error bars plotted on the shadow areas represent the ZDCFs. One can see in Figure 2 that the calculated cross-correlation functions through the two methods give almost the same results. The centroids of CEDCFs are located at +4.4 days, +7.1 days, and +13.6 days, while those of ZDCFs are found at +6.6 days, +7.1 days, and +5.1 days for the three pairs, respectively. A positive time lag indicates that the soft X-rays are delayed with respect to hard X-rays in this paper, These results indicate the existence of day-scale soft lags in Cen A.

To evaluate the statistical uncertainties of the soft lags, we performed Monte-Carlo simulations utilizing the FR/RSS method. For constructing CCCDs, we calculated CEDCF for 1000 light curves produced by Monte-Carlo simulations with a bin size of 2 days. In order to minimize the systematic effect of bin size, we performed similar calculations with 3, 4, and 5 day bins, and consequently a total of 4000 simulations are performed to obtain a distribution of centroids. In the same manner as those for CEDCF, we also performed simulations for smoothed ZDCF calculated by using running average of 2, 3, 4, and 5 points, where we selected $n_{\text{min}} = 11$ for each simulated ZDCF in this analysis. The distributions of the centroid of CEDCFs and smoothed ZDCFs are presented in Figure 3. Solid lines show the obtained CCCDs derived through the CEDCF method, and dotted lines show the obtained CCCDs built by ZDCF method. On the basis of these distributions, we calculated the 1σ error ranges of the soft lags. The obtained results are consistent between two methods. Table 1 shows the magnitudes of the soft lags and associated 1σ error estimated. The first column gives the energy bands used for the calculation, the second and fourth gives the possible lag obtained by the

Energy band (keV)	$\tau_{\text{cent}}^{\text{CEDCF}}$ (days)	$P_{>0}^{\text{CEDCF}}$ (days)	$\tau_{\text{cent}}^{\text{ZDCF}}$ (day)	$P_{>0}^{\text{ZDCF}}$ (days)
2–4 vs 4–10	$6.5^{+8.1}_{-6.2}$	0.85	$6.1^{+5.7}_{-5.5}$	0.86
4–10 vs 10–20	$6.5^{+7.9}_{-6.4}$	0.84	$5.4^{+7.3}_{-6.6}$	0.80
2–4 vs 10–20	$13.6^{+7.2}_{-8.0}$	0.97	$11.7^{+8.4}_{-7.6}$	0.96

Table 1. The estimated soft lags during MJD = 55075–55160 using FR/RSS for CEDCF and ZDCF methods. In this analysis, CEDCFs are calculated with one day intervals and n_{min} is confined to 11 for calculating ZDCF. The details of these methods are written in the text.

CCCD of CEDCF $\tau_{\text{cent}}^{\text{CEDCF}}$ and ZDCF $\tau_{\text{cent}}^{\text{ZDCF}}$. We also show the probability that the true lag is larger than zero, where soft lag is represented as positive. These results indicate the existence of statistically significant day-scale soft lags during this flare of Cen A.

4.2 Flare profile fitting

To connect the soft lags to physical phenomena, we tried to model the three light curves. For simplicity, we adopt a model consisting of a flare lying on a slowly varying base line flux for each energy band. First, we estimate the base line component by fitting a quadratic function to the data in the range of $\text{MJD} < 55080$ and $55135 < \text{MJD}$. After subtracting the best-fit quadratic model from the light curves, we fit a flare model function to the data at $55080 \leq \text{MJD} \leq 55135$. In accordance with Abdo et al. (2010a), we used the following function as the flare model:

$$F(t) = 2F_0 \left(e^{\frac{t_0-t}{T_r}} + e^{-\frac{t_0-t}{T_d}} \right)^{-1}, \quad (9)$$

where F_0 is the amplitude of the flare, t_0 determines the peak epoch, and T_r and T_d are the rise and decay times. In order to obtain a robust flare profile while minimizing the effect of small fluctuations that cannot be interpreted by the simple model, the fit was performed by using `n1rob` function in the “robust base” package of “R”. This function fits a nonlinear regression model to the data by robust M-estimators (Huber, 1964) using the iteratively re-weighted least squares method. The modeled light curves composed of the best-fit base lines are shown in Figure 1. The best-fit parameters of the flares and the corresponding 68% confidence intervals are summarized in Table 2. The uncertainties are derived from distributions of the parameters constructed by 5000 Monte-Carlo simulations with assumption that the errors in the observed fluxes have normal distribution. For the flares in 2–4 keV and 4–10 keV, one can see that the rise time T_r and the epoch of the peak t_0 are almost the same while the decay time T_d is appreciably different; *i.e.*, T_d in 2–4 keV is longer than that in 4–10 keV by about 9 days. This difference is comparable to the soft lag between 2–4 keV and 4–10 keV (6–7 day) estimated from DCF. On the other hand, the flare profile in 10–20 keV looks somewhat different

Energy (keV)	F_0 (mCrab)	t_0	T_r (day)	T_d (day)
2–4	$5.9^{+2.6}_{-0.8}$	$55086.2^{+1.5}_{-1.4}$	$1.4^{+1.3}_{-0.7}$	$20.3^{+13.0}_{-8.8}$
4–10	$18.1^{+4.2}_{-2.4}$	$55086.3^{+1.6}_{-0.8}$	$1.6^{+0.9}_{-0.7}$	$11.0^{+6.4}_{-4.8}$
10–20	$26.2^{+13.8}_{-3.8}$	$55083.5^{+0.9}_{-0.5}$	$0.3^{+0.4}_{-0.2}$	$10.6^{+10.5}_{-5.6}$

Table 2. The best-fit parameters of the flare profiles in three energy bands obtained with the robust fitting method. The 68% confidence intervals are also shown.

from the others. The shorter rise time implies that the high energy photons are emitted from a smaller region than that of low energy photons. For the decay time, the shortest value is found in 10–20 keV. The soft lag between 2–4 keV and 10–20 keV (12–14 days) obtained with DCF corresponds to the sum of the differences of the peak time t_0 (~ 3 days) and the decay time T_d (~ 10 days) in these energy bands.

5 Discussion

Our analysis results indicate the existence of the soft lag in X-ray variation. The result of the flare profile fitting suggests that the flare decaying time (expressed as T_d in §4.2) makes the major contribution to the soft lags. In the following sections, we discuss if the observed soft lags are accountable by the energy-dependent decay times under two X-ray emission models for AGNs, namely, the one-zone synchrotron self-Compton process in the jet, and the Compton up-scattering of the disk photons in the corona.

5.1 One-zone synchrotron self-Compton

Soft lags in AGNs are sometimes explained by the radiative cooling of relativistic electrons through the one-zone synchrotron self-Compton (SSC) process (*e.g.* Kataoka et al. 2000). In this model, the power produced by a single electron in the synchrotron radiation and the inverse Compton scattering of a single electron is given by (Rybicki & Lightman 1979)

$$P = \frac{d}{dt}[(\gamma - 1)m_e c^2] = \frac{4}{3}c\sigma_T(\gamma^2 - 1)(U_B + U_{\text{ph}}), \quad (10)$$

where m_e is the mass of an electron, σ_T is the Thomson cross section, and U_B and U_{ph} are the energy densities of magnetic field ($B^2/8\pi$) and the seed photon field, respectively. The cooling timescale, which sets the characteristic timescale for the losing kinetic energy of electrons by the synchrotron radiation and the inverse Compton scattering, can be expressed as follows:

$$t_{\text{cool}} = \frac{(\gamma - 1)m_e c^2}{4c\sigma_T(\gamma^2 - 1)(U_B + U_{\text{ph}})/3} = \frac{3m_e c}{4\sigma_T(\gamma + 1)(U_B + U_{\text{ph}})} \quad (11)$$

The time lag (t_{lag}) of emission at γ_2 with respect to emission at γ_1 is the time it takes for electrons to lose energy equal to $\gamma_1 - \gamma_2$. Thus, t_{lag} is given by

$$t_{\text{lag}} = \frac{3m_e c}{4\sigma_T(U_B + U_{\text{ph}})} \left(\frac{1}{\gamma_2 + 1} - \frac{1}{\gamma_1 + 1} \right). \quad (12)$$

In this paper, we consider the upper limit of the cooling time of an electron:

$$t_{\text{lag}} < \frac{3m_e c}{4\sigma_T U_B} \frac{1}{\gamma_{\text{min}} + 1}, \quad (13)$$

where γ_{min} is the minimum Lorentz factor of electrons in the emission region. Abdo et al. (2010b) attempted to explain the multi-wavelength SED of Cen A with the one zone SSC model and yielded the magnetic field of the emitting region $B = 6.2$ G and a minimum electron Lorentz factor $\gamma_{\text{min}} = 300$. Assigning these values to Eq.(13), we obtain < 1.1 day which is an upper limit of radiative cooling time of the electrons in the emission region. The obtained limitation is inconsistent with the observed soft lags and the decay times of the flares.

When we accept that the following five simplifications: (1) the photons before scattering have a single energy (ϵ_0), (2) Lorentz factors of electrons producing X-ray photons ($\gamma_{2-4\text{keV}}$, $\gamma_{4-10\text{keV}}$, and $\gamma_{10-20\text{keV}}$) are substantially larger than unity ($1/\gamma \approx 0$), (3) the energies of the photons after scattering are $\gamma^2 \epsilon_0$, (4) Lorentz factors are in the ratios $\gamma_{2-4\text{keV}} : \gamma_{4-10\text{keV}} : \gamma_{10-20\text{keV}} = 1 : \sqrt{7/3} : \sqrt{5}$ corresponding to the ratios of the square roots of the means of the observed energy ranges, and (5) $U_B \gg U_{\text{ph}}$ due to Klein-Nishina effect, then Eq.(12) provides the product of two parameters $\gamma_{2-4\text{keV}} U_B = 20.3$ as the most likely value to interpret the soft lags listed in Table 1. In Figure 4, we present 68% and 90% confidence interval in the $\gamma_{2-4\text{keV}} - B$ plane derived from the distribution of the simulated soft lags (described in §4.1). The set of parameters $B = 6.2$ G and $\gamma_{\text{min}} = 300$ based on one zone SSC model is located at outside the 99% confidence range (Figure 4). Although weaker B field or lower γ_{min} (or both) may produce the obtained soft lags, studies of SEDs variation of blazars suggest that the B and γ_{min} do not change significantly even during flares (*e.g.* Donnarumma et al. 2009, Vercellone et al. 2010, Rani et al. 2011). This inconsistency implies that the X-ray radiation from Cen A and its variability cannot be explained by the simple one zone SSC model.

5.2 Up-scattered black body radiation

Next, we discuss an alternative scenario in which the origin of the observed X-ray radiation is the soft seed photons up-scattered in a optically thin corona on (or surrounding) the accretion disk. Assuming that the soft seed photons are provided by the blackbody radiation in the standard accretion disk, and the disk temperature (T_{eff}) is locally constant, we can describe U_{ph} using Stefan-Boltzmann law as

$$U_{\text{ph}} = \frac{\Omega}{4\pi} \times aT_{\text{eff}}^4, \quad (14)$$

where $a = 7.56 \times 10^{-15} \text{ erg cm}^{-3} \text{ K}^{-4}$ is the radiation constant, and Ω is the solid angle of the region of blackbody emission viewed from the corona. In the standard disk model, the disk temperature at given radius R from the central black hole is given by

$$T(R) = \left[\frac{3G\dot{M}M_{\text{BH}}}{8\pi R^3\sigma} \left\{ 1 - \left(\frac{R_{\text{in}}}{R} \right)^{\frac{1}{2}} \right\} \right]^{\frac{1}{4}}, \quad (15)$$

where G is the gravitational constant, \dot{M} is a mass accretion rate, σ is the Stefan-Boltzmann constant, and R_{in} is the innermost radius of the accretion disk (Shakura & Sunyaev 1973). This function has a maximum value when the radius at $R = (7/6)^2 R_{\text{in}}$. The numerical value of the maximum disk temperature based on Eq.(15) is expressed as a function of R_{in} measured in unit of the Schwarzschild radius $R_s = 2GM_{\text{BH}}/c^2$:

$$T_{\text{max}} \approx 2.5 \times 10^5 \left(\frac{M_{\text{BH}}}{10^8 M_{\odot}} \right)^{-\frac{1}{2}} \left(\frac{\dot{M}}{1 M_{\odot}/\text{yr}} \right)^{\frac{1}{4}} \left(\frac{R_{\text{in}}}{R_s} \right)^{-\frac{3}{4}} \text{ K}. \quad (16)$$

Employing values of $M_{\text{BH}} = 2.0 \times 10^8 M_{\odot}$ (Marconi et al. 2001), $\dot{M} = 6.4 \times 10^{-4} M_{\odot}/\text{yr}$ inferred by spherical (Bondi) accretion (Evans et al. 2004), and $3R_s$ as R_{in} which is the innermost stable circular orbit (ISCO) around a Schwarzschild black hole, we obtain the approximate upper limit of the standard accretion disk temperature of Cen A to be $T_{\text{max}} = 1.2 \times 10^4 \text{ K}$ ($\approx 1 \text{ eV}$). In addition, if we presume that the soft lag of 2–4 keV versus 10–20 keV obtained with the CEDCF method (=13.6 days; see Table 1 in §4) is the lower limit of the electrons' Compton cooling time in the corona, we can find a more strict constraint of the effective temperature of the accretion disk as $T_{\text{eff}} \leq 8.3 \times 10^3 \text{ K}$ ($\approx 0.7 \text{ eV}$) by using Eqs.(11) and (14) with considering $\gamma \geq 1$ and setting $\Omega = 2\pi$ and $U_B = 0$. This upper limit of the disk temperature is substantially lower than other Seyfert galaxies (10–50 eV; Petrucci et al. 2001), though it is quite reasonable when we consider the low Eddington-scaled accretion rate $\dot{m} \approx 10^{-4}$ (Soria et al. 2006).

In black hole binaries (BHBs), the disk is truncated at a larger radius than ISCO in the quiescent state (Esin et al. 2001). Similarly we can expect the temperature of the standard accretion disk in AGNs becomes lower as mass accretion rate decreases. The limit of $T_{\text{eff}} \lesssim 0.7 \text{ eV}$ corresponding to $R_{\text{in}} \gtrsim 5R_s$ is then plausible. Although it is difficult to estimate the accurate Lorentz factors of the electrons producing observed X-ray photons, the observed day-scale soft lags can be explained by the difference of the Compton cooling time of electrons with different energies in the Comptonizing plasma. Moreover, the flare decaying time in the 2–4 keV band (~ 20 days) is consistent with the break time scale of the power spectrum density (PSD) in the 1.5–12 keV band ($T_b = 18.3_{-6.7}^{+18.3}$ days; Rothschild et al. 2011). Ishibashi and Courvoisier (2012) argued that the PSD break in the X-ray band of AGNs represents the cooling time of the electrons in the Comptonization process in the non-

relativistic limit. These argument supports our interpretation that the flare decay time is the cooling time of the corona.

On the other hand, Beckmann et al. (2011) found an electron temperature $kT_e = 206$ keV (corresponds to $\gamma = 1.4$) by fitting the hard X-ray spectrum with a thermal Comptonization model (compPS) assuming an inner disk temperature of $T_{\text{bb}} = 10$ eV (fixed). We note that the assumed disk temperature is inconsistent with our limit $T_{\text{eff}} \lesssim 0.7$ eV. For this assumed temperature $T_{\text{bb}} = 10$ with $\Omega = 2\pi$ and $U_B = 0$, we obtain 3×10^{-4} days as the typical cooling time of the plasma, that is much smaller than the observed soft lags and the flare decay times. This inconsistency might imply that a different set of parameters or another spectral model are required for the observed flare.

6 Summary

Employing the DCF methods, we found soft lags on a time scale of days between all energy bands' X-ray variation in 2–4 keV, 4–10 keV, and 10–20 keV of Centaurus A in the X-ray light curve observed by *MAXI*, and confirmed that the soft lags are statistically significant by performing Monte-Carlo simulations known as FR/RSS. With the flare profile fitting, we find that the soft lag is mainly due to the longer flare decay time in lower energy bands than that in higher energy bands. We assumed that these decay times reflect the cooling timescale of electrons associated with X-ray radiation process. If the observed X-rays are emitted by SSC in a single zone in the jet with the parameters ($B = 6.2$ G, $\gamma_{\text{min}} = 300$) given by Abdo et al. (2010b), the day-scale soft lags cannot be explained because of too short cooling time of highly energetic electrons. For interpreting the evaluated soft lags by the simple one zone SSC model, a weaker B field or a smaller Lorentz factor of electrons (or both) are required. On the other hand, assuming that the X-rays originate in the disk photons which are up-scattered by electrons in the corona around the accretion disk, we constrain the effective temperature of the accretion disk ($\lesssim 0.7$ eV), and then we show that the observed lags can be explained by the difference in the energy-dependent cooling times of the electrons in the corona. The plausibility of this scenario is supported by the consistency in the fare decay times and the break timescale of the power spectrum density.

References

- Abdo, A., et al. 2010a, ApJ, 716, 835
 Abdo, A., et al. 2010b, ApJ, 719, 1433
 Alexander, T., et al. 1997, Astronomical Time Series, eds. D. Maoz, A. Sternberg, & E. M. Leibowitz, 1997

(Dordrecht: Kluwer), 163

- Beckmann, V., et al. 2011, *A&A*, 531, 70
- Chiaberge, M., et al. 2001, *MNRAS*, 324, L33
- De Marco, B., et al. 2013, *MNRAS*, 431, 2441
- Donnarumma, I., et al. 2009, *ApJ*, 707, 1115
- Edelson, R. A. & Krolic, J. H., 1988, *ApJ*, 333, 646
- Esin, A. A., et al. 2001, *ApJ*, 555, 483
- Evans, D. A., et al. 2004, *ApJ*, 612, 786
- Fukazawa, Y., et al. 2011, *ApJ*, 743, 124
- Gil-Merino, R., Wisotzki, L., & Wambsganss, J. 2002, *A&A*, 381, 428
- Goicoechea, L., et al. 1998, *ApJ*, 492, 74
- Harris, G. L. H., et al., 2010, *PASA*, 27, 457
- Huber, P. J. 1964, *Annals of Mathematical Statistics*, 35, 73
- Hiroi, K., et al. 2011, *PASJ*, 63, S677
- Hiroi, K., et al. 2013, *ApJS*, 207, 36
- Ishibashi, W & Courvoisier T. J.-L., 2012, *A&A*, 540, L2
- Kataoka, J., et al., 2000, *ApJ*, 528, 243
- Matsuoka, M., et al. 2009, *PASJ*, 61, 999
- Marconi, A., et al. 2001, *ApJ*, 549, 915
- Mihara, T., et al. 2011, *PASJ*, 63, 623
- Morganti, R., et al. 1992, *MNRAS*, 256, 1
- Peterson, M., et al. 1998, *PASP*, 110, 660
- Petropoulou, M., et al. 2013, *A&A*, 562, 11
- Petrucci, P. O., et al. 2001, *ApJ*, 556, 716
- Rani, B., et al. 2011, *MNRAS*, 417, 1881
- Rybicki, G. B., & Lightman, A. P. 1979, *Radiative Processes in Astrophysics*, ed. Rybicki, G. B., & Lightman
- Rothschild, R., et al. 1999, *ApJ*, 510, 651
- Rothschild, R., et al. 2011, *ApJ*, 733, 23
- Roustazadeh, P., & Böttcher, M. 2011, *ApJ*, 728, 134
- Shakura, N. I. & Sunyaev, R. A. 1973, *A&A*, 24, 337
- Soria, R., et al., 2006, *ApJ*, 640, 126
- Sriram, K., et al., 2009, *ApJ*, 700, 1042
- Sugizaki, M., et al., 2011, *PASJ*, 63, 635
- Tanihata, C., et al., 2001, *ApJ*, 563, 569

Tingay, S. J., et al. 1998, AJ, 115, 960
Tomida, H., et al. 2011, PASJ, 63, 397
Tueller, J., et al. 2008, ApJ, 681, 113
Vercellone, S., et al. 2010, ApJ, 712, 405

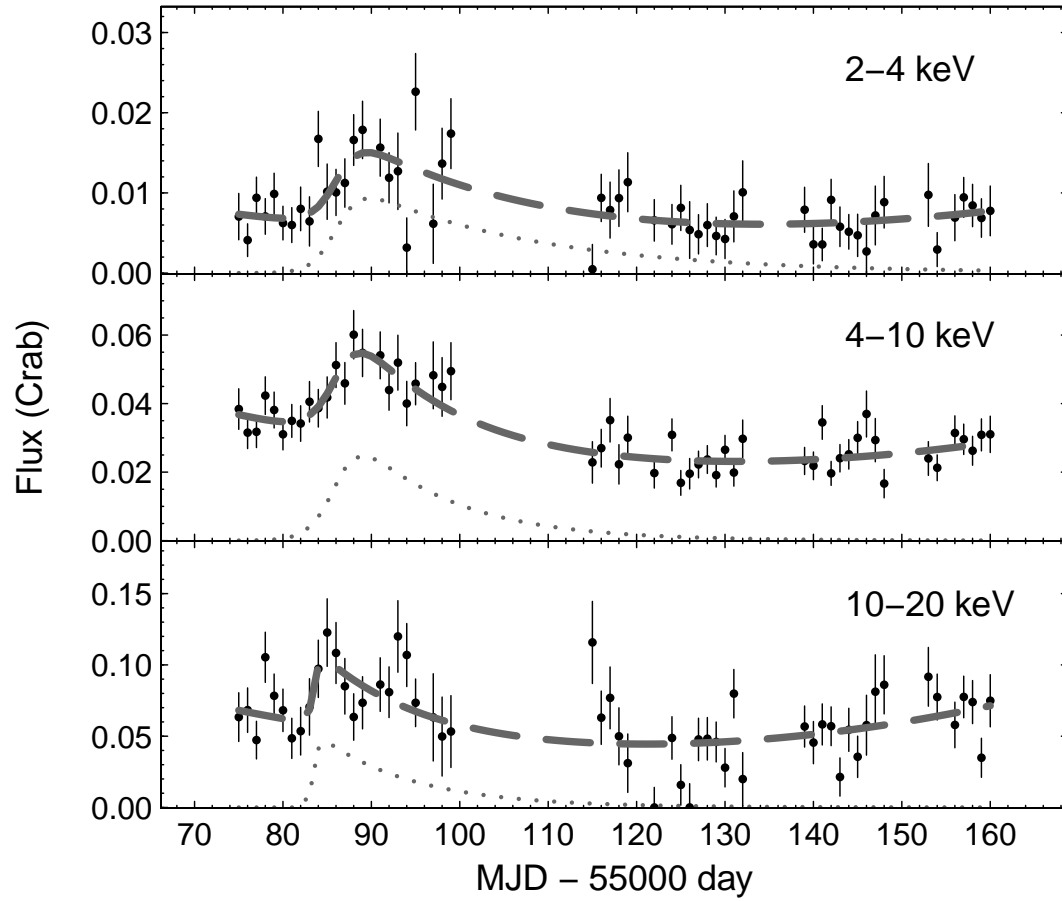


Fig. 1. X-ray light curves of Centaurus A obtained by the MAXI/GSC. The obtained flux data are plotted as the black points with error bars. The error bars present 1σ errors derived from C -statistics (see Hiroi et al. 2011 for details). the thick gray dashed curves correspond to the modeled light curves, and thin grey dotted curves represent flares decomposed (see §4.2).

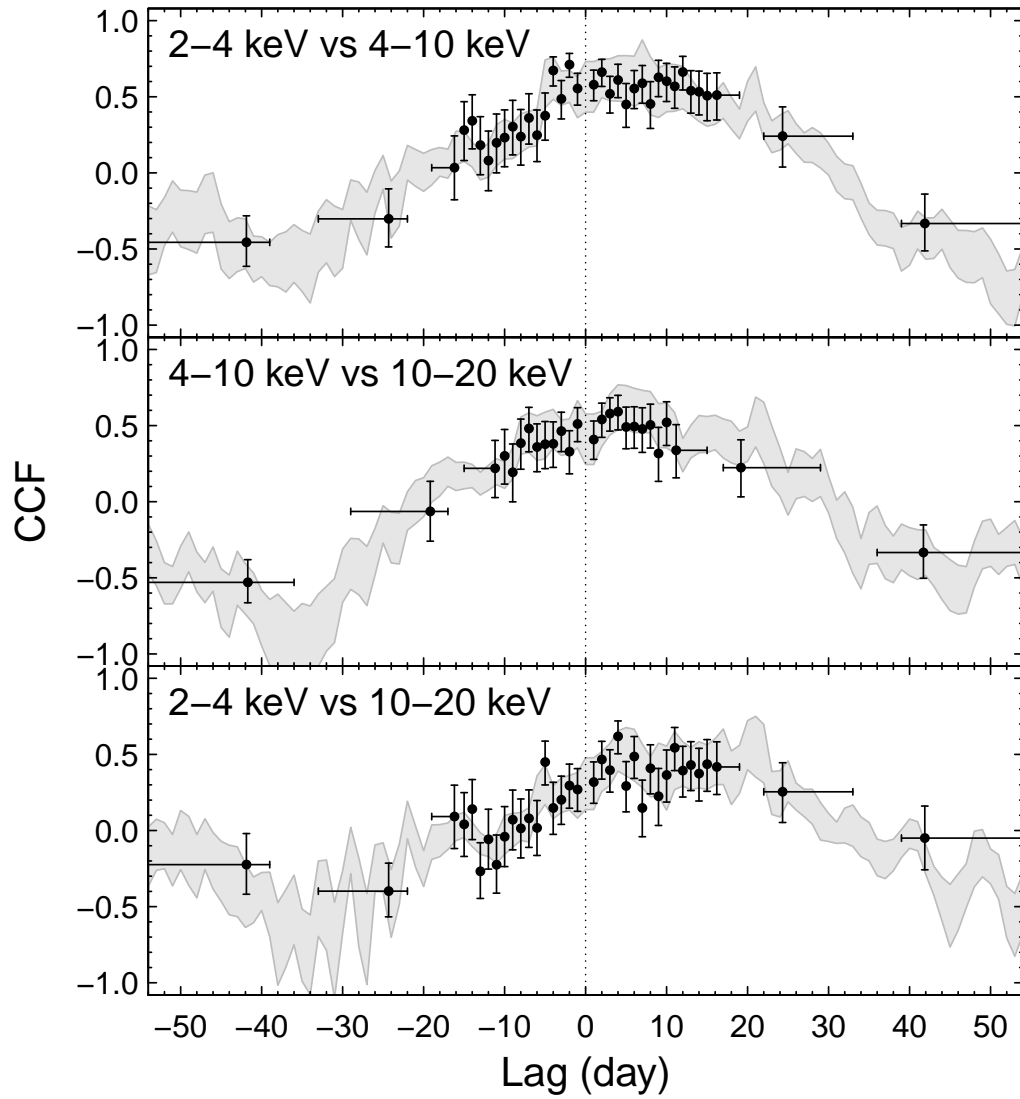


Fig. 2. CEDCFs and ZDCFs calculated between 2–4 keV versus 4–10 keV, 4–10 keV versus 10–20 keV, and 2–4 keV versus 10–20 keV. CEDCFs are shown as gray shadowed area, and ZDCFs are plotted by black circles with error bars. Dashed vertical line stands for $\tau_{\text{lag}} = 0$.

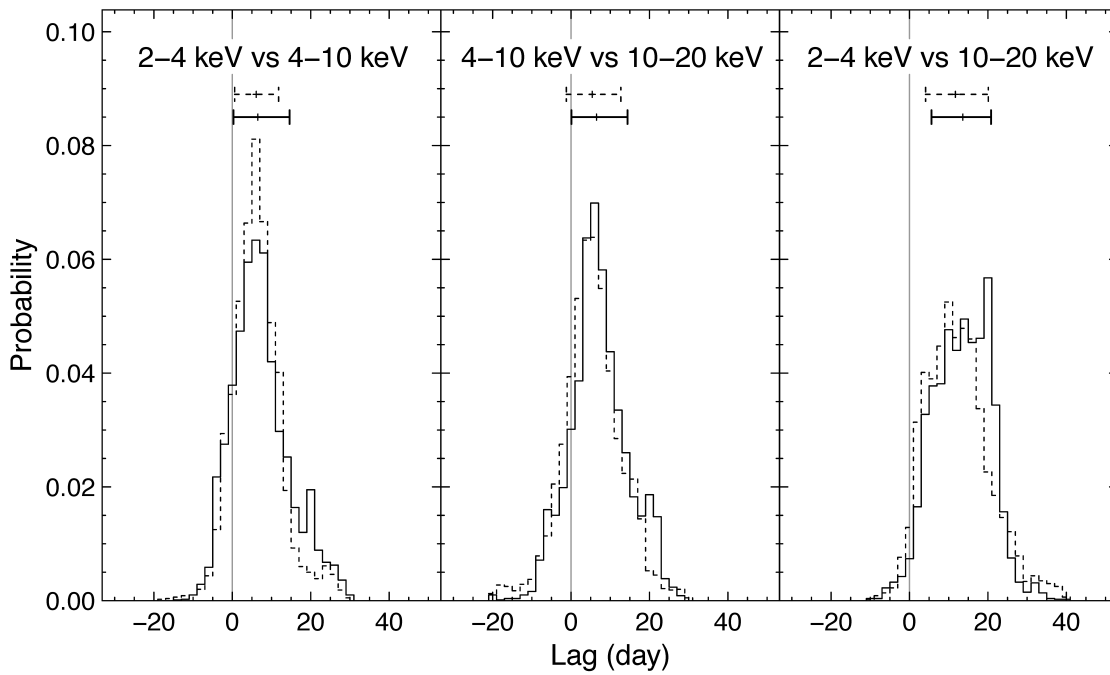


Fig. 3. Cross correlation centroid distributions (CCCDs) of CEDCF (solid line) and ZDCF (dashed line) obtained by running FR/RSS Monte-Carlo simulations. Derived soft lags and corresponding 1σ ranges are also shown above the histograms. Gray vertical lines are drawn at $\tau_{\text{lag}} = 0$.

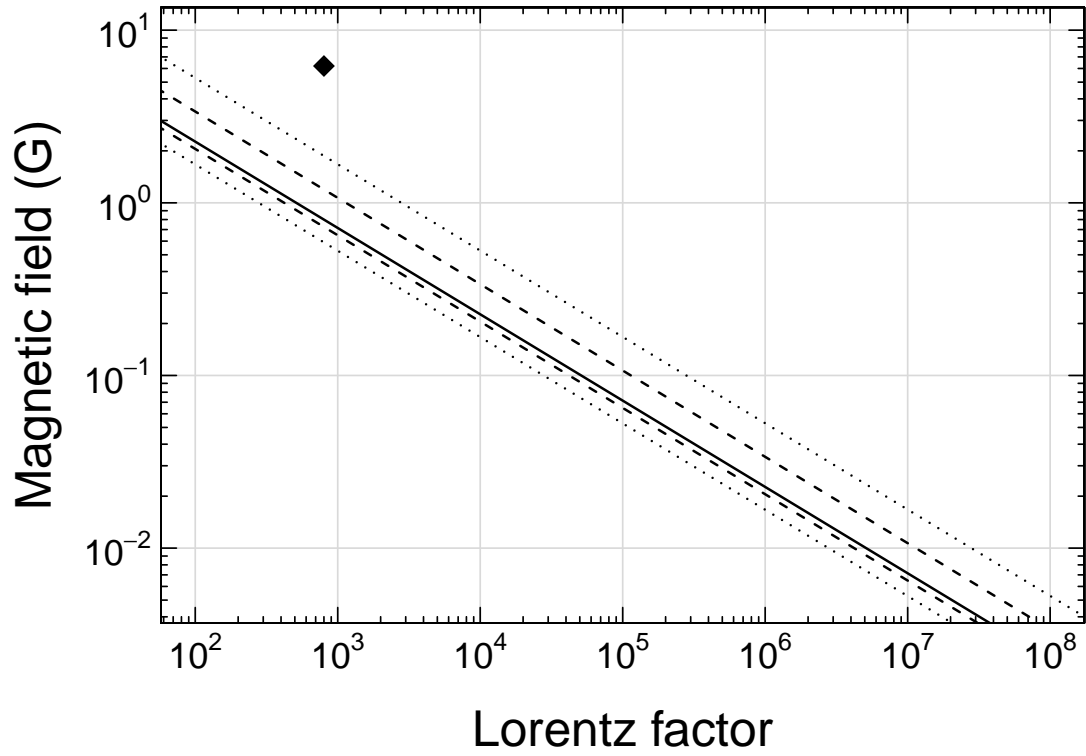


Fig. 4. The 68% and 90% confidence intervals in the $\gamma - B$ plane derived from fitting the model based on Eq.(12) to simulated soft lags described in §4.1. We also show the best-fit value for the obtained soft lags by the solid line. The rhombic data point denotes the parameter set (γ_{\min}, B) given by Abdo et al. (2010b).